frontiers | Frontiers in Chemistry

TYPE Original Research
PUBLISHED 28 September 2023
DOI 10.3389/fchem.2023.1259000

OPEN ACCESS

EDITED BY
Gunter Heymann,
University of Innsbruck, Austria

REVIEWED BY
Hubert Huppertz,
University of Innsbruck, Austria
Miriding Mutailipu,
Chinese Academy of Sciences (CAS), China

*CORRESPONDENCE
Irina Chuvashova,
irina.chuvashova@fiu.edu
Olga Ibragimova,
oibra005@fiu.edu

RECEIVED 14 July 2023
ACCEPTED 05 September 2023
PUBLISHED 28 September 2023

CITATION
Ibragimova O, Vaquero L, Hussein Z, Drozd V, Chariton S, Prakapenka V and Chuvashova I (2023), The synthesis of novel lanthanum hydroxyborate at extreme conditions.
Front. Chem. 11:1259000.
doi: 10.3389/fchem.2023.1259000

The synthesis of novel lanthanum hydroxyborate at extreme conditions

Olga Ibragimova[1]*, Lia Vaquero[1], Zain Hussein[2], Vadym Drozd[3], Stella Chariton[4], Vitali Prakapenka[4] and Irina Chuvashova[1,2]*

[1]Department of Chemistry and Biochemistry, Florida International University, Miami, FL, United States, [2]Physics Department, Florida International University, Miami, FL, United States, [3]Department of Mechanical and Materials Engineering, Florida International University, Miami, FL, United States, [4]Center for Advanced Radiation Sources, The University of Chicago, Chicago, IL, United States

The novel structure of lanthanum hydroxyborate $La_2B_2O_5(OH)_2$ was synthesized by the reaction of partially hydrolyzed lanthanum and boron oxide in a diamond anvil cell under high-pressure/high-temperature (HPHT) conditions of 30 GPa and ~2,400 K. The single-crystal X-ray structure determination of the lanthanum hydroxyborate revealed: $P\bar{3}c1$, a = 6.555(2) Å, c = 17.485(8) Å, Z = 6, R_1 = 0.056. The three-dimensional structure consists of discrete planar BO_3 groups and three crystallographically different La ions: one is surrounded by 9, one by 10, and one by 12 oxygen anions. The band gap was estimated using *ab initio* calculations to be 4.64 eV at ambient pressure and 5.26 eV at 30 GPa. The current work describes the novel HPHT lanthanum hydroxyborate with potential application as a deep-ultraviolet birefringent material.

KEYWORDS

high pressure, high temperature, synthesis, birefringence, lanthanum borate, rare-earth borates, new compound, diamond anvil cell

1 Introduction

In recent decades, borates have garnered significant interest as versatile materials due to their varied crystal structures, impressive linear and nonlinear optical (NLO) properties, and favorable machining characteristics (Chen et al., 1995; Wu et al., 1996; Chénais et al., 2002; Jia et al., 2017; Zou and Ok, 2020; Guo et al., 2022). Notably, considerable research efforts have been devoted to the development of novel borate-based birefringent materials for potential application in the deep-ultraviolet (DUV) region (longer wavelength portion of UV-C; 190 nm ≤ λ_0 ≤ 280 nm; 4.43 eV ≤ E_0 ≤ 6.53 eV) (Zhang et al., 2020).

Despite the different principles in crystal symmetries of NLO and birefringent materials, sufficiently large optical anisotropy plays a crucial role in the applications for both types (Guo et al., 2022). It is widely recognized that the small double refraction of NLO crystals limits their ability to achieve the shortest phase-matching wavelength, thereby negatively affecting potential applications in the DUV region (Jiang et al., 2015). Birefringent materials play an important role in modulating light polarization in the optical communication and laser industries (Li and Ma, 2012). Several commercially available crystals like calcite (Ghosh, 1999), YVO_4 (DeShazer, 2002), α-BaB_2O_4 (Guoqing et al., 1998; Solntsev et al., 2002), and MgF_2 (Dodge, 1984) have found utility in the optical spectrum spanning from the infrared (IR) to the UV range with wavelengths below 400 nm. However, these four compounds are not suitable for application in the DUV region because:

- The low transmittance in the DUV range of α-BaB_2O_4, calcite, and YVO_4 restricts their application in shorter-wavelength regions;
- An extremely small birefringence (Δn = 0.0128 at 235.7 nm) limits the application of MgF_2 in the DUV region (Scott, 1962; Dodge, 1984).

Consequently, an ideal crystal must possess high transmittance in the DUV range, large birefringence (Δn > 0.08) (Gong et al., 2020), and a short UV cutoff edge (the smaller the better) (Guo et al., 2022). Today, the scarcity of such materials meeting these criteria underscores the importance of exploring novel DUV crystals with substantial birefringence.

In terms of borates, there are three basic groups that form unique structures: linear BO_2, trigonal-planar BO_3 and tetrahedral BO_4, which occur as discrete oxyanions or polymerize to form finite clusters, chains, sheets, and frameworks. Anionic group theory gives the understanding of structure-property relationships. The key factor that affects optical properties is if the anionic unit is capable to produce a wide band gap, high polarizability anisotropy, and hyperpolarizability (Huang et al., 2021; Mutailipu et al., 2021). The triangle π-conjugated BO_3 group has the largest hyperpolarizability (β_{max} = 10.80) among BO_2 (β_{max} = 0) and BO_4 (β_{max} = 3.61), and a good relation between the other two parameters: band gap (E_g = 8.48 eV) and polarizability anisotropy (δ = 7.01) (Mutailipu et al., 2021). The birefringence originates from the dependence of dipole oscillators and refractive index, and it can be considered as a result of the functional unit`s arrangement (Wang F. et al., 2021). Therefore, the solution for the large optical anisotropy lies in metal cations and the type of functional anion (Jin et al., 2021). The metal cations can form MO_n polyhedra with large deformability and thereby increase the optical anisotropy (Wu et al., 2019). But with the positive influence on birefringence, there is a negative effect on DUV transmittance: the crystals with big metal cations have a smaller band gap and as a consequence may hardly transmit in the DUV spectral region. The birefringence is not sensitive to the exact orientation of the BO_3 groups because it is almost optically isotropic within the BO_3 plane (Chen et al., 2012). It was shown that all borates crystal structures with only triangle borate groups could be divided into three structural types according to the arrangement of these groups: 1) the BO_3 planes arranged in a nearly coplanar pattern, 2) in a coaxial pattern, 3) and in the other inclined patterns (Jiang et al., 2015). The crystals with coplanar arrangement generally have the largest birefringence, while those with disordered patterns have the smallest (Jiang et al., 2014; Lin et al., 2014).

Along with alkali and transition metals borates, rare-earth (RE) borates (and lanthanum borates in particular) have raised significant interest due to their stable physical and chemical properties, wide bandwidth, and good light transmittance. The system La-B-O is represented by several compositionally different borates: λ-$LaBO_3$ (Sari et al., 2017), high-temperature modification H-$LaBO_3$, LaB_3O_6 (ambient pressure), and its two high-pressure modifications γ-LaB_3O_6 (Emme et al., 2004) and δ-LaB_3O_6 (Heymann et al., 2006), $La_4B_{14}O_{27}$ (Nikelski et al., 2008), $La_{26}O_{27}(BO_3)_8$ (Lin et al., 1996), $La_4B_{10}O_{21}$ (isotypic to $Pr_4B_{10}O_{21}$) (Hinteregger et al., 2012) and $La_2B_8O_{15}$ (isotypic to $Ce_2B_8O_{15}$) (Glätzle et al., 2016). Except for the high-pressure modifications (γ-LaB_3O_6, δ-LaB_3O_6, and $La_4B_{10}O_{21}$), all known lanthanum borates are synthesized by heating stoichiometric mixtures of La_2O_3 and B_2O_3 under ambient pressure conditions. However, this simple synthesis fails to produce pure crystalline phases (Shmyt'ko et al., 2013). Hence, HPHT synthesis serves as a viable alternative. There is a common trend in high-pressure borates where the boron atoms tend to prefer four-fold coordination as pressure increases. Typically, trigonal-planar BO_3 groups transform into tetrahedral BO_4 groups beyond 10 GPa pressure (Hinteregger et al., 2012). However, a few compounds are known to contain trigonal-planar BO_3 groups beyond this pressure threshold, for example, in $Ho_{31}O_{27}(BO_3)_3(BO_4)_6$ (Hering et al., 2010).

In the present study, we have applied methods of single-crystal X-ray diffraction in laser-heated diamond anvil cell (DAC) to synthesize lanthanum hydroxyborate $La_2B_2O_5(OH)_2$ for the first time and characterize its crystal structure. We performed *ab initio* calculations of the band gap and compared both: the band gap and its structural properties with literature. The structural organization of $La_2B_2O_5(OH)_2$ allows us to propose that the lanthanum borates with isolated BO_3 groups can be used as a potential DUV birefringent material.

2 Materials and methods

2.1 Sample preparation

For the synthesis, we used a non-stoichiometric mixture of partially hydrolyzed La (a piece of lanthanum 99.9% purity from Fisher Scientific left on humid air for 3 days) and B_2O_3 (99.999% purity, purchased from Fisher Scientific), finely grounded and pre-pressed into pellets between two diamonds. The pre-pressed pellet of size 10*15*5 μm^3 was loaded in the symmetric DAC (Symm100 by Almax EasyLab) equipped with Boehler–Almax diamonds with a 200 μm culet size. Rhenium gasket was pre-indented to the thickness of 26 μm, and a hole with the diameter of about 110 μm was drilled with a laser-drilling system at GeoSoilEnviroCARS (GSECARS), Advanced Photon Source (APS), Argonne National Laboratory (ANL). A 4 μm piece of gold and a 15 μm ruby ball (DACtools, LLC) were used as pressure calibrants (Ye et al., 2018). Neon was loaded using the COMPRES/GSECARS gas loading system available at APS (Rivers et al., 2008) and served as a pressure-transmitting medium.

2.2 Laser-heating experiments

Double-sided laser-heating experiments coupled with X-ray diffraction (XRD) measurements were conducted at the 13ID-D beamline at GSECARS of the APS, ANL. The laser heating system at the beamline is equipped with two 1,064 nm wavelength infrared lasers that produce a flat-top spot size of around 10 μm in diameter (full width at half-maximum) (Goncharov et al., 2010). We used double-sided laser heating in the burst mode with a heating duration of 1 or 3 s, collecting XRD of the sample during and after heating. The surface temperatures of both sides were measured by the standard spectroradiometry method (Heinz and Jeanloz, 1987)

using an IsoPlane SCT 320 spectrometer with a PI-MAX3 1024i ICCD camera from Princeton Instruments.

The DAC was compressed stepwise to a maximum pressure of 30(1) GPa and laser-heated at 3.3(5) and 13.3(5) GPa to a maximum temperature of 2,285(325) and 2,430(130) K, respectively. After each heating cycle, a detailed X-ray diffraction map was collected around the heated spot in order to determine the occurrence of the reaction and the phase composition. At each pressure point, single crystal X-ray diffraction images were collected in a few spots with decent quality for phase composition determination.

2.3 X-ray data analysis

The crystal structures of the sample in the DAC were investigated through *in situ* XRD measurements using synchrotron radiation performed at the 13ID-D beamline of the APS, ANL. A monochromatic X-ray beam of 42 keV (λ = 0.2952 Å) was used to collect powder and single crystal data on a Pilatus 1M CdTe large area detector.

2.3.1 Powder diffraction

Powder collection was performed as a single image in the omega scanning range of ±20° with an exposure time of 40 s. Detector parameters were calibrated using LaB_6.

The data for powder analysis was prepared and converted into the required file extension using Dioptas software (Prescher and Prakapenka, 2015). Powder XRD data analysis consisted of structure refinement by the Le Bail method using the GSAS II software (Toby and Von Dreele, 2013).

2.3.2 Single crystal diffraction

Single crystal collection included 120 frames in the omega scanning range of ±34° with a step of 0.5° and an exposure time of 1 s per step. Sample-to-detector distance, coordinates of the beam center, tilt angle, and tilt plane rotation angle of the detector images were calibrated using an orthoenstatite crystal.

Single-crystal XRD data (unit cell determination, integration of the reflection intensities, absorption corrections) were processed using CrysAlisPro software (Rigaku Oxford Diffraction, 2019). For the search of the domains during data reduction, the DAFi software was used (Aslandukov et al., 2022). The structure was determined by SHELXT (Sheldrick, 2015), a structure solution package that uses the method of intrinsic phasing. The crystal structure was refined against F^2 on all data by full-matrix least-squares using SHELXL software (Sheldrick, 2015). SHELXT and SHELXL were implemented in the Jana2006 software package (Petříček et al., 2014). Crystal structure visualization was made using VESTA (Momma and Izumi, 2011) and Diamond software (Putz and Brandenburg, 1999).

Because more than 50% of the diffraction reflections were blocked by the body of the diamond anvil cell, the data sets of the reflections were incomplete. To improve the data/parameter ratio, only the atomic thermal parameters of lanthanum and oxygen were refined using anisotropic approximation, leading to an R_1 value of 5.6%. Due to the presence of high-Z lanthanum atoms, the residual electron density peaks were on the order of 2–6 e/Å^3, which is comparable with the number of electrons in boron and oxygen atoms. Assignment of the residual density peaks to boron or oxygen atoms did not improve the final R-values, and therefore, the high residuals likely originate from the incompleteness of the XRD data sets. The typical data/parameter ratios were on the order of 10–15. The detailed summary of the crystal structure refinement, along with unit cell parameters, atomic coordinates, and atomic displacement parameters, is shown in Table 1 and Supplementary Tables S1, S2.

TABLE 1 Crystal data and structure refinement parameters for $La_2B_2O_5(OH)_2$.

Empirical formula	$La_2B_2O_5(OH)_2$
Crystal system	Trigonal
Space group	$P\bar{3}c1$
Space group number	165
a (Å)	6.556(2)
c (Å)	17.485(9)
V (Å^3)	650.8(5)
Z	6
R_{int}	0.06
R_1	0.056
GOF (obs)	1.82
GOF (all)	1.42
# reflections (total)	764
# of refinable parameters	46

2.4 Scanning electron microscopy

The composition of the sample mixture prior to loading in the DAC was analyzed by means of scanning electron microscopy using the JOEL JSM-IT500HR scanning electron microscope (JEOL USA, Inc., Peabody, MA, United States). The chemical composition was checked at 15 kV using energy-dispersive X-ray spectroscopy (EDS) of QUANTAX EDS System with XFlash 6160 detector (Bruker Nano GmbH, Berlin, Germany). No impurities or traces of any other elements were found. The detailed summary is shown in Supplementary Figure S1.

2.5 Band gap calculations

Density functional theory (DFT) calculations were performed using Vienna *ab initio* simulation package (VASP 6.3) (Kresse and Furthmüller, 1996a; Kresse and Furthmüller, 1996b). Local Density Approximation (LDA) and Generalized Gradient Approximation (GGA) were used to describe exchange and correlation effects. Electron wave functions were expanded by plane wave with a cutoff energy of 520 eV. Monkhorst-Pack (Monkhorst and Pack, 1976) *k*-point grids were set as 12 × 12 × 4 for the structure relaxation and 24 × 24 × 8 for the electronic structure calculations. Atomic relaxation was performed until the change

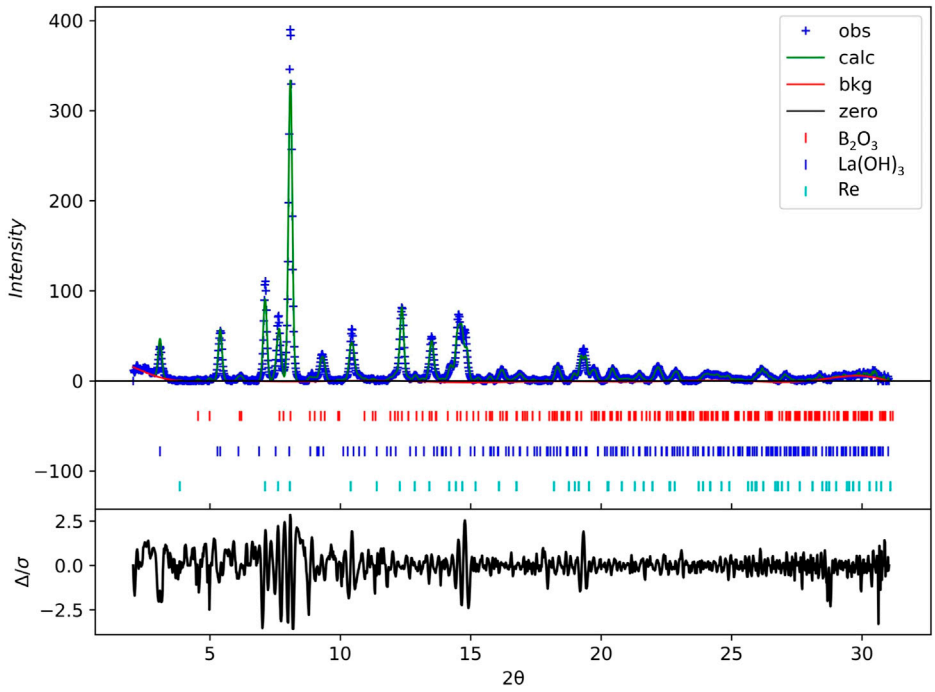

FIGURE 1
Powder XRD pattern of the mixture prior to heating at 3.3(5) GPa: blue crosses are experimental data from this study, the green line corresponds to the calculated curve, the red one represents the background, and the black one shows the difference between observed and calculated curves. The ticks represent the different phases: red is B_2O_3 (ICSD 16021), blue is $La(OH)_3$ (ICSD 239411), and teal one is Re (ICSD 291898).

in the electronic and ionic steps were less than 10^{-6} and 10^{-5} eV, respectively. VASPKIT package (Wang V. et al., 2021) was used to extract and analyze the VASP raw output files. Calculations were performed at ambient pressure and external pressure of 30.0 GPa.

3 Results

The synthesis of new lanthanum hydroxyborate was performed from the mixture of partially hydrolyzed lanthanum powder and boron oxide. The initial mixture has irregular composition (insert in Supplementary Figure S1). As lanthanum can oxidize on air to either oxide, hydroxide, carbonate, or hydroxycarbonate depending on the conditions and humidity, we performed EDS analysis to confirm the composition of starting mixture. The brief inspection of the EDS spectrum of the initial mixture shows that the sample is composed of the elements La, B, and O. We used carbon tape as a sample mount which may account for the carbon present in the spectra.

To confirm the composition of the initial mixture, we performed powder XRD analysis at the pressure of 3.3(5) GPa. The powder pattern can be found in Figure 1. There are characteristic peaks of $La(OH)_3$, B_2O_3, and Re. The unit cell parameters for $La(OH)_3$ ($P6_3/m$) are: a = 6.506(4) Å, c = 3.8673(7) Å, V = 141.75(12) Å^3; for B_2O_3 ($P3_1$) are: a = 4.3789(11) Å, c = 8.2888(16) Å, V = 137.64(5) Å^3; and for Re ($P6_3/mmc$) are: a = 2.716(7) Å, c = 4.396(30) Å, V = 28.09(20) Å^3. The R-factor is equal to 0.6%. Thus, the source of lanthanum in the system was lanthanum hydroxide. Our sample is very close to the gasket; therefore, the presence of rhenium is not surprising. No characteristic peaks of other compounds exist, such as lanthanum carbonate, lanthanum hydroxycarbonate, or lanthanum oxycarbonate. We did not observe the characteristic peaks of various lanthanum borate phases either. As a result, we can rule out the possibility of a reaction occurring during compression at 3.3(5) GPa without heating.

Laser heating up to 2,285(325) K at 3.3(5) GPa led to a pressure jump to 6.6(5) GPa, however, the reaction did not occur. Data collection at 13.3(5) GPa before and after heating to 2,430(130) K did not produce good-quality crystalline samples either. Fortunately, the diffraction pattern after increasing pressure up to 30(1) GPa confirmed the chemical reaction by forming a new, previously unknown structure.

By employing single crystal diffraction analysis, the new compound crystallizes in the centrosymmetric trigonal space group $P\bar{3}c1$ (no. 165) with lattice parameters a = 6.555(2) Å, c = 17.485(8) Å (Table 1). It consists of a dense, three-dimensional network (Figure 2) composed of planar triangles of BO_3 connected with three crystallographically independent lanthanum ions. The lanthanum atoms possess different coordination spheres (Supplementary Figure S2): La01 is coordinated by 10 oxygen atoms, La02 is coordinated by 12 oxygen atoms, and La03 is coordinated by 9 oxygen atoms. The distances La-O are in the range of 2.27(2)–2.614(12) Å. The B-O bond lengths are in the range of 1.26(2)–1.321(15) Å (for all bond lengths in the structure, see Supplementary Table S3). These bond distances are slightly smaller than those published for alkali- and rare-earth borates which can be explained by the higher pressure reached during this experiment.

As the amount of water absorbed by the lanthanum is unknown, for the structure solution, we used only three elements: La, B, and O. According to the structure refinement, our formula ended up as $La_2B_2O_7$. To achieve charge balance, instead of two oxygen atoms,

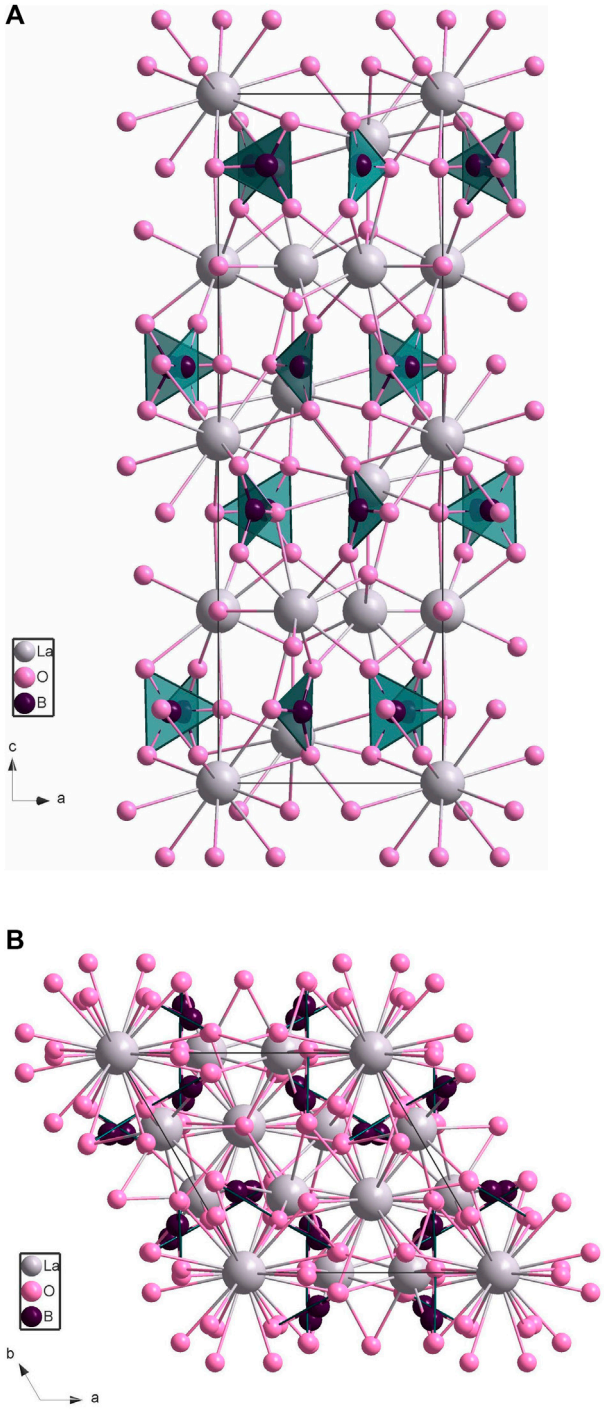

FIGURE 2
Crystal structure of $La_2B_2O_5(OH)_2$ (hydrogen atoms are not shown): **(A)** along *a* axis, **(B)** along *c* axis. Lanthanum atoms are shown in grey, oxygens are pink, and boron atoms are in the center of each planar triangle and are shown in dark purple.

there should be two hydroxyl groups. This agrees well with our XRD data of the starting compositions. Therefore, the new borate has a composition of $La_2B_2O_5(OH)_2$.

The band gap calculated by DFT method is 3.40 eV (GGA)/4.64 eV (LDA) at ambient pressure and 5.31 eV (GGA)/5.26 eV (LDA) at 30 GPa pressure (Figure 3 for LDA and Supplementary Figure S4 for GGA). These values correspond to the short cutoff edge in the range from 365 to 233 nm. Commonly, the GGA and LDA method-based calculations tend to slightly underestimate the band gap, therefore the real value might be slightly higher and, consequently, the cutoff edge smaller (Bagayoko, 2014; Baiheti et al., 2021).

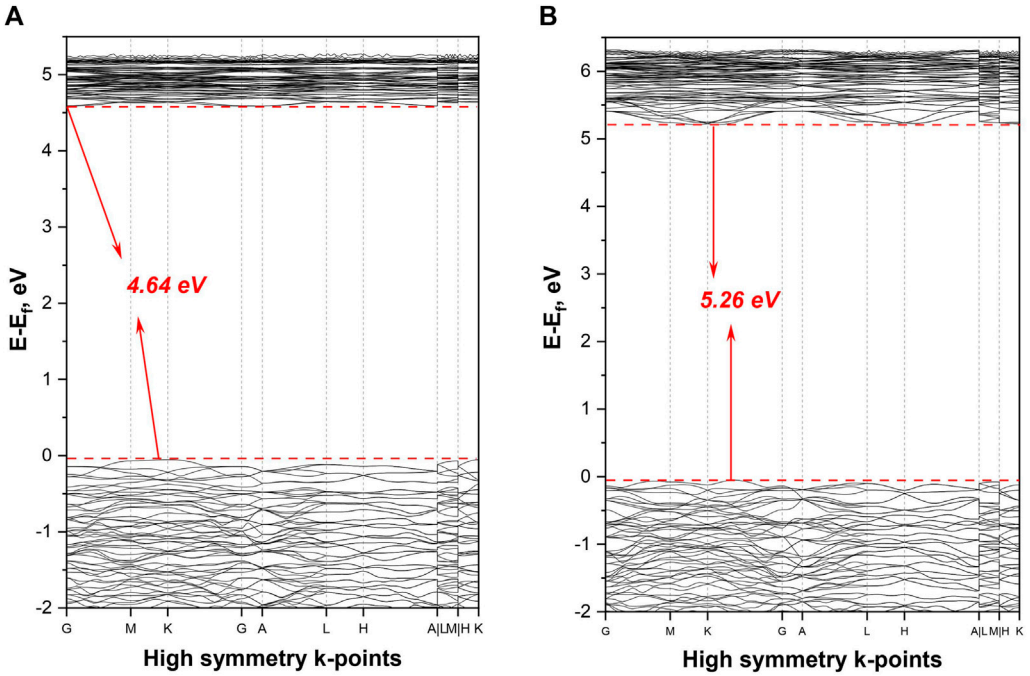

FIGURE 3
The electronic band structure calculated by using LDA method: **(A)** for ambient pressure, and **(B)** for 30 GPa.

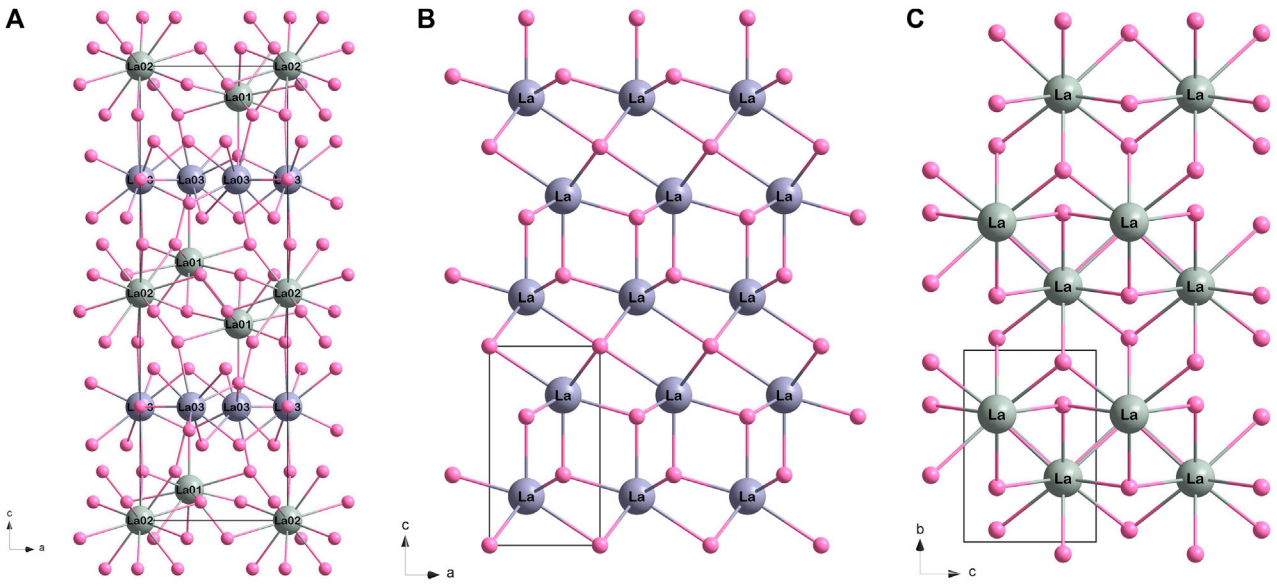

FIGURE 4
The comparison of La-O frame (hydrogen and boron atoms are not shown) for: **(A)** $La_2B_2O_5(OH)_2$ (present work), **(B)** La_2O_3 (ICSD 56771), and **(C)** $La(OH)_3$ (ICSD 239411). For convenience, the lanthanum atoms with different pattern are shown in different shades of grey: for La_2O_3 pattern in violetish grey, for $La(OH)_3$ pattern in greenish grey.

4 Discussion

The starting mixture for the reaction consisted of $La(OH)_3$ and B_2O_3. During laser heating up to 2,430(130) K, the hydroxide partially decomposed to La_2O_3 and H_2O without subsequent melting of La_2O_3 [$T_{m\ (amb)}$ = 2588 K (Grundy et al., 2000)], while boron oxide melted [$T_{m\ (8\ GPa)}$ ~ 1,800 K (Solozhenko et al., 2015)]. The behavior of B_2O_3 melt is similar to SiO_2, and it readily dissolves metallic oxides with the formation of borates (Huppertz, 2011), so the lanthanum borate was

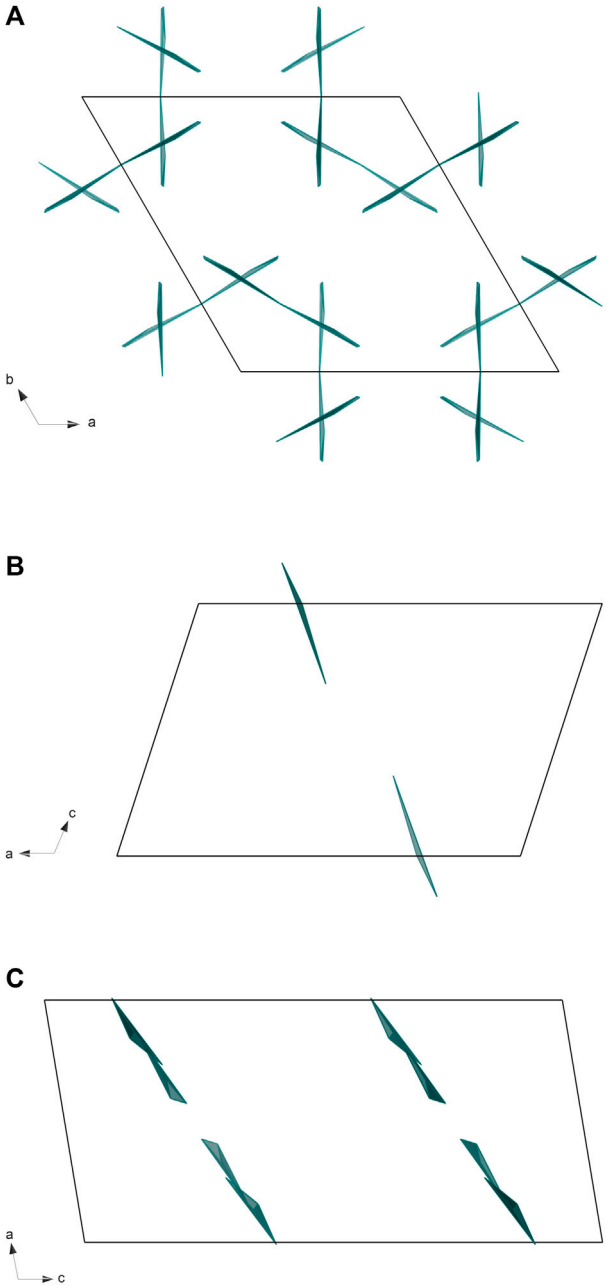

FIGURE 5
The comparison of BO_3 polyhedra arrangement for: **(A)** $La_2B_2O_5(OH)_2$ (present work), **(B)** H-$LaBO_3$ (ICSD 15383), and **(C)** $La_{26}(BO_3)_8O_{27}$ (ICSD 82308). For convenience, only BO_3 polyhedra are shown.

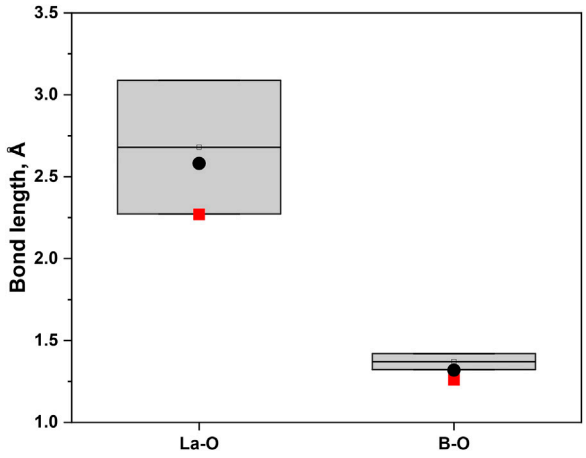

FIGURE 6
The comparison of the bond distances for La-O and B-O (in trigonal planar orientation) from publications (Böhlhoff et al., 1971; Lin et al., 1996; Emme et al., 2004; Hinteregger et al., 2012) and for $La_2B_2O_5(OH)_2$ (present work). The ranges from the literature are shown in grey bars, the red squares are corresponding to the smallest value of the bond length of the $La_2B_2O_5(OH)_2$, while the black dots are representing the biggest value.

synthesized by dissolving La_2O_3 and $La(OH)_3$ in B_2O_3 with subsequent reaction.

The structure of $La_2B_2O_5(OH)_2$ is based on La-O layers identical to those in the A-type La_2O_3 structure ($P\bar{3}m$) and $La(OH)_3$ ($P6_3/m$) (Figure 4). During HP synthesis, the lanthanum-oxygen layers of $La(OH)_3$ were integrated between similar layers of La_2O_3. The oxide layers are rotated by 180° relative to each other along the *c* axis. The coordination numbers for La in $La(OH)_3$ frame increase from 9 to 10 and 12 [La01 and La02 in $La_2B_2O_5(OH)_2$]; while for La in La_2O_3 pattern—from 7 to 9 [La03 in $La_2B_2O_5(OH)_2$]. Boron atoms have three-fold coordination and are located in the cavities between La01/02-O and La03-O layers. The positional disorder of the BO_3 groups is unusual for known RE borates and has never been described before. In terms of a three-fold coordinated boron atom, in RE borates BO_3 group can form either linked chains [for example, in α-$Sm(BO_3)_2$ (Fuchs et al., 2020a) or in LaB_2O_4F (Hinteregger et al., 2013b)], or isolated triangles [for instance, in $NdBO_3$ (Müller-Bunz et al., 2003) or in $Dy_5(BO_3)_2F_9$ (Hinteregger et al., 2013a)]. The arrangement of boron groups in most cases is coplanar (parallel to one plane) or slightly distorted. In $La_2B_2O_5(OH)_2$ boron groups have a coaxial arrangement: each BO_3 triangle occupies one of three possible positions along C_3 axis and lies in the glade *n* plane (Supplementary Figure S5). BO_3 group exhibits C_2 symmetry as it represents an isosceles triangle.

There are known structures of RE hydroxyborates, for example, high-pressure $La_3B_6O_{13}(OH)$ (Fuchs et al., 2020b), and $LaB_2O_4(OH)$ (Bashir et al., 2017). However, both are composed of edge-sharing BO_4 tetrahedra which distinguishes them from the newly synthesized $La_2B_2O_5(OH)_2$. We found only two lanthanum borates with similar structure: H-$LaBO_3$ (Böhlhoff et al., 1971) and $La_{26}(BO_3)_8O_{27}$ (Lin et al., 1996). Both these structures consist of repeated La-O and BO_3 patterns: the orientation of planar BO_3 groups in H-$LaBO_3$ is coplanar, while in $La_{26}(BO_3)_8O_{27}$ the BO_3 groups have a slightly distorted arrangement (Figure 5). The bond distances in $La_2B_2O_5(OH)_2$ correspond well to typical bond lengths in lanthanum borates (Figure 6). For example, in comparison with $La_{26}(BO_3)_8O_{27}$ at ambient pressure where the bond distances for La-O are in the range 2.272(10)–3.047(9) Å, and for B-O are in the range 1.34(2)–1.42(2) Å (Lin et al., 1996), the newly synthesized $La_2B_2O_5(OH)_2$ at 30(1) GPa have the bond lengths 2.27(2)–2.612(14) Å and 1.26(2)–1.319(15) Å for La-O and B-O, respectively.

While the borates with parallel arrangement of planar BO_3 groups have the largest birefringence (Jiang et al., 2015), the

situation with coaxial BO_3 arrangement is slightly different. The value for optical anisotropy depends not only on BO_3 pattern, but also on the detailed orientation and spatial density of the planar BO_3 groups (Jiang et al., 2015). Additionally, the presence of hydroxyl anions linked with isolated triangular boron groups may enlarge the birefringence by delocalization of π electrons (Jin et al., 2021). Our calculated band gap values for ambient [3.40 eV (GGA)/4.64 eV (LDA)] and high pressure [5.31 eV (GGA)/ 5.26 eV (LDA)] are typical for lanthanum borates with three-fold coordinated boron. For example, the calculated (GGA) and experimental band gap at ambient conditions for $LaBO_3$ with two-dimensional BO_3 layers are 4.81 and 5.23 eV (Sha et al., 2021) respectively. As mentioned earlier, the presence of rare-earth elements may positively affect the birefringence but at the same time decreases the band gap. As we are looking at the combination of factors, there is a good probability that synthesized $La_2B_2O_5(OH)_2$ has high birefringence with the cutoff edge short enough to transmit in the longer wavelength portion of UV-C.

5 Conclusion

During the HPHT synthesis at 30(1) GPa and 2,430(130) K, we were able to obtain a new structure of lanthanum hydroxyborate [$La_2B_2O_5(OH)_2$] with planar BO_3 groups. In contrast with the most known RE borates (including high-pressure structures), $La_2B_2O_5(OH)_2$ does not form a B-O framework and does not have BO_4 tetrahedra: trigonal-planar BO_3 groups occupy the cavities between La-O layers and create the coaxial pattern. The estimated band gap for lanthanum hydroxyborate is 4.64 eV (for ambient pressure) and 5.26 eV (for 30 GPa), which fits well into the acceptable range for DUV transparency. The structural organization of $La_2B_2O_5(OH)_2$ and its electronic properties allows us to propose that this class of lanthanum borates can be used as a potential DUV birefringent material.

Data availability statement

The datasets presented in this study can be found in online repositories. The names of the repository/repositories and accession number(s) can be found below: the joint CCDC/FIZ Karlsruhe online deposition service: https://www.ccdc.cam.ac.uk/structures/; the deposition number CSD-2280897.

Author contributions

OI: Investigation, Conceptualization, Data curation, Software, Visualization, Writing–original draft. LV: Investigation, Writing–review and editing. ZH: Investigation, Writing–review and editing. VD: Writing–review and editing, Resources, Software. SC: Methodology, Supervision, Writing–review and editing. VP: Methodology, Supervision, Writing–review and editing. IC: Methodology, Supervision, Writing–review and editing, Funding acquisition, Investigation, Project administration, Data curation, Validation.

Funding

The authors declare financial support was received for the research, authorship, and/or publication of this article. Funding was provided by Florida International University.

Acknowledgments

This research used resources of the Advanced Photon Source, a U.S. Department of Energy (DOE) Office of Science User Facility operated for the DOE Office of Science by Argonne National Laboratory under Contract No. DE-AC02-06CH11357. We acknowledge the support of GeoSoilEnviroCARS (Sector 13), which is supported by the National Science Foundation—Earth Sciences (EAR-1634415). This work used Bridges-2 at Pittsburgh Supercomputing Center through allocation Discover MAT230033 from the Advanced Cyberinfrastructure Coordination Ecosystem: Services and Support (ACCESS) program, which is supported by National Science Foundation grants #2138259, #2138286, #2138307, #2137603, and #2138296. The Bridges-2 system is supported by NSF award number ACI-1928147, at the Pittsburgh Supercomputing Center (PSC) (Towns et al., 2014). The authors are grateful to Florida International University for financial support.

Conflict of interest

The authors declare that the research was conducted in the absence of any commercial or financial relationships that could be construed as a potential conflict of interest.

Publisher's note

Supplementary material

The Supplementary Material for this article can be found online at: https://www.frontiersin.org/articles/10.3389/fchem.2023.1259000/full#supplementary-material

References

Aslandukov, A., Aslandukov, M., Dubrovinskaia, N., and Dubrovinsky, L. (2022). Domain auto finder (DAFi) program: the analysis of single-crystal X-ray diffraction data from polycrystalline samples. *J. Appl. Crystallogr.* 55 (5), 1383–1391. doi:10.1107/S1600576722008081

Bagayoko, D. (2014). Understanding density functional theory (DFT) and completing it in practice. *AIP Adv.* 4 (12). doi:10.1063/1.4903408

Baiheti, T., Han, S., Jin, W., Yang, Z., and Pan, S. (2021). $Cs_2AlB_5O_{10}$: a short-wavelength nonlinear optical crystal with moderate second harmonic generation response. *Dalton Trans.* 50 (3), 822–825. doi:10.1039/D0DT04020G

Bashir, B., Zhang, B., Lee, M.-H., Pan, S., and Yang, Z. (2017). DFT-based comparative study about the influence of fluorine and hydroxyl anions on optoelectric properties of borate crystals: Choice for better anion. *Inorg. Chem.* 56 (10), 5636–5645. doi:10.1021/acs.inorgchem.7b00120

Böhlhoff, R., Bambauer, H. U., and Hoffmann, W. (1971). Die kristallstruktur von Hoch-$LaBO_3$. *Z. fur Kristallogr.* 133 (1-6), 386–395. doi:10.1524/zkri.1971.133.16.386

Chen, C., Sasaki, T., Li, R., Wu, Y., Lin, Z., Mori, Y., et al. (2012). *Nonlinear optical borate crystals*. John Wiley & Sons, 15–115.

Chen, C., Wang, Y., Xia, Y., Wu, B., Tang, D., Wu, K., et al. (1995). New development of nonlinear optical crystals for the ultraviolet region with molecular engineering approach. *J. Appl. Phys.* 77 (6), 2268–2272. doi:10.1063/1.358814

Chénais, S., Druon, F., Balembois, F., Georges, P., Gaumé, R., Haumesser, P. H., et al. (2002). Spectroscopy and efficient laser action from diode pumping of a new broadly tunable crystal: Yb:$Sr_3Y(BO_3)_3$. *J. Opt. Soc. Am. B* 19 (5), 1083. doi:10.1364/JOSAB.19.001083

DeShazer, L. G. (2002). "Improved midinfrared polarizers using yttrium vanadate," in *Polarization analysis and measurement IV, proc. SPIE 4481* (SPIE). doi:10.1117/12.452881

Dodge, M. J. (1984). Refractive properties of magnesium fluoride. *Appl. Opt.* 23 (12), 1980. doi:10.1364/AO.23.001980

Emme, H., Despotopoulou, C., and Huppertz, H. (2004). High-pressure synthesis and crystal structure of the structurally new orthorhombic rare-earth Meta-oxoborates γ-$RE(BO_2)_3$ (RE = La - Nd). *Z. Fur Anorg. Und Allg. Chem.* 630 (13–14), 2450–2457. doi:10.1002/zaac.200400202

Fuchs, B., Heymann, G., Wang, X., Lkhamsuren Bayarjargal, A. T., Siegel, R., Schmutzler, A., et al. (2020a). $La_3B_6O_{13}(OH)$: The first acentric high-pressure borate displaying edge-sharing BO_4 tetrahedra. *Chem. – A Eur. J.* 26 (30), 6851–6861. doi:10.1002/chem.201905419

Fuchs, B., Kindler, R. O., Heymann, G., and Huppertz, H. (2020b). High-pressure synthesis and crystal structure of the samarium meta-oxoborate γ-$Sm(BO_2)_3$. *Z. Für Naturforsch. B* 75 (6–7), 589–595. doi:10.1515/znb-2020-0045

Ghosh, G. (1999). Dispersion-equation coefficients for the refractive index and birefringence of calcite and quartz crystals. *Opt. Commun.* 163 (1–3), 95–102. doi:10.1016/S0030-4018(99)00091-7

Glätzle, M., Hoerder, G. J., and Huppertz, H. (2016). $RE_2B_8O_{15}$ (RE = La, Pr, Nd) - syntheses of three new rare earth borates isotypic to $Ce_2B_8O_{15}$. *Zeitschrift Fur Naturforschung - Sect. B J. Chem. Sci.* 71 (5), 535–542. doi:10.1515/znb-2016-0027

Gong, P., Kang, L., and Lin, Z. (2020). Realizing deep-ultraviolet second harmonic generation by first-principles-guided materials exploration in hydroxyborates. *J. Am. Chem. Soc.* 142 (35), 15157–15163. doi:10.1021/jacs.0c07256

Grundy, A. N., Hallstedt, B., and Gauckler, L. J. (2000). Thermodynamic assessment of the lanthanum-oxygen system. *J. Phase Equilibria* 22, 105–113. doi:10.1361/105497101770338950

Guo, R., Jiang, X., Guo, S., Xia, M., Liu, L., Lin, Z., et al. (2022). Realization of enlarged birefringence from $BaCdBe_2(BO_3)_2F_2$ to $NaMgBe_2(BO_3)_2F$ via the cation size effect as a potential deep-ultraviolet birefringent material. *Inorg. Chem.* 61 (19), 7624–7630. doi:10.1021/acs.inorgchem.2c00880

Guoqing, Z., Jun, X., Xingda, C., Heyu, Z., Siting, W., Ke, X., et al. (1998). Growth and spectrum of a novel birefringent α-BaB_2O_4 crystal. *J. Cryst. Growth* 191 (3), 517–519. doi:10.1016/S0022-0248(98)00162-6

Heinz, D. L., and Jeanloz, R. (1987). "Temperature measurements in the laser-heated diamond cell," in *High-pressure research in mineral physics: A volume in honor of syun-iti akimoto*. Editors M. H. Manghnani and Y. Syono (Terra Scientific Publishing Company). doi:10.1029/GM039p0113

Hering, S. A., Haberer, A., Kaindl, R., and Huppertz, H. (2010). High-pressure synthesis and crystal structure of the new holmium oxoborate $Ho_{31}O_{27}(BO_3)_3(BO_4)_6$. *Solid State Sci.* 12 (12), 1993–2002. doi:10.1016/j.solidstatesciences.2010.08.016

Heymann, G., Soltner, T., and Huppertz, H. (2006). δ-$La(BO_2)_3$ (≡δ-LaB_3O_6): A new high-pressure modification of lanthanum meta-oxoborate. *Solid State Sci.* 8 (7), 821–829. doi:10.1016/j.solidstatesciences.2006.03.002

Hinteregger, E., Böhler, G., Hofer, T. S., and Huppertz, H. (2013a). High-pressure syntheses and characterization of the rare earth borates $RE_5(BO_3)_2F_9$ (RE=Dy, Ho). *Z. Für Naturforsch. B* 68 (1), 29–38. doi:10.5560/znb.2013-2313

Hinteregger, E., Heymann, G., Hofer, T. S., and Huppertz, H. (2012). High-pressure synthesis and characterization of the rare-earth borate $La_4B_{10}O_{21}$. *Z. Für Naturforsch. B* 67b, 605–613. doi:10.5560/znb.2012-0001

Hinteregger, E., Kocsis, K., Hofer, T. S., Heymann, G., Perfler, L., and Huppertz, H. (2013b). High-pressure synthesis and characterization of the rare-earth fluoride borate LaB_2O_4F. *Z. Fur Naturforsch. B* 68 (9), 951–959. doi:10.5560/ZNB.2013-3177

Huang, C., Mutailipu, M., Zhang, F., Griffith, K. J., Hu, C., Yang, Z., et al. (2021). Expanding the chemistry of borates with functional $[BO_2]^-$ anions. *Nat. Commun.* 12 (1), 2597. doi:10.1038/s41467-021-22835-4

Huppertz, H. (2011). New synthetic discoveries via high-pressure solid-state chemistry. *Chem. Commun.* 47 (1), 131–140. doi:10.1039/c0cc02715d

Jia, Z., Zhang, N., Ma, Y., Zhao, L., Xia, M., and Li, R. (2017). Top-seeded solution growth and optical properties of deep-UV birefringent crystal $Ba_2Ca(B_3O_6)_2$. *Cryst. Growth Des.* 17 (2), 558–562. doi:10.1021/acs.cgd.6b01428

Jiang, X., Kang, L., Luo, S., Gong, P., Lee, M.-H., and Lin, Z. (2014). Development of nonlinear optical materials promoted by density functional theory simulations. *Int. J. Mod. Phys. B* 28 (27), 1430018. doi:10.1142/S0217979214300187

Jiang, X., Luo, S., Kang, L., Gong, P., Huang, H., Wang, S., et al. (2015). First-principles evaluation of the alkali and/or alkaline earth beryllium borates in deep ultraviolet nonlinear optical applications. *ACS Photonics* 2 (8), 1183–1191. doi:10.1021/acsphotonics.5b00248

Jin, C., Shi, X., Zeng, H., Han, S., Chen, Z., Yang, Z., et al. (2021). Hydroxyfluorooxoborate $Na[B_3O_3F_2(OH)_2]\cdot[B(OH)_3]$: Optimizing the optical anisotropy with heteroanionic units for deep ultraviolet birefringent crystals. *Angew. Chem. - Int. Ed.* 60 (37), 20469–20475. doi:10.1002/anie.202107291

Kresse, G., and Furthmüller, J. (1996a). Efficiency of *ab-initio* total energy calculations for metals and semiconductors using a plane-wave basis set. *Comput. Mater. Sci.* 6 (1), 15–50. doi:10.1016/0927-0256(96)00008-0

Kresse, G., and Furthmüller, J. (1996b). Efficient iterative schemes for *ab initio* total-energy calculations using a plane-wave basis set. *Phys. Rev. B* 54 (16), 11169–11186. doi:10.1103/PhysRevB.54.11169

Li, R. K., and Ma, Y. (2012). Chemical engineering of a birefringent crystal transparent in the deep UV range. *CrystEngComm* 14 (17), 5421. doi:10.1039/c2ce25240f

Lin, J. H., Su, M. Z., Wurst, K., and Schweda, E. (1996). The structure of $La_{26}(BO_3)_8O_{27}$: A structure with a distorted fluorite type arrangement of atoms. *J. Solid State Chem.* 126 (2), 287–291. doi:10.1006/jssc.1996.0339

Lin, Z., Jiang, X., Kang, L., Gong, P., Luo, S., and Lee, M.-H. (2014). First-principles materials applications and design of nonlinear optical crystals. *J. Phys. D Appl. Phys.* 47 (25), 253001. doi:10.1088/0022-3727/47/25/253001

Momma, K., and Izumi, F. (2011). VESTA 3 for three-dimensional visualization of crystal, volumetric and morphology data. *J. Appl. Crystallogr.* 44 (6), 1272–1276. doi:10.1107/S0021889811038970

Monkhorst, H. J., and Pack, J. D. (1976). Special points for Brillouin-zone integrations. *Phys. Rev. B* 13 (12), 5188–5192. doi:10.1103/PhysRevB.13.5188

Müller-Bunz, H., Nikelski, T., and Schleid, T. (2003). Einkristalle des Neodym(III)-meta-Borats $Nd(BO_2)_3$ und -ortho-Borats $Nd[BO_3]$/Single Crystals of the Neodymium(III) meta-Borate $Nd(BO_2)_3$ and ortho-Borate $Nd[BO_3]$. *Z. Für Naturforsch. B* 58 (5), 375–380. doi:10.1515/znb-2003-0503

Mutailipu, M., Poeppelmeier, K. R., and Pan, S. (2021). Borates: A rich source for optical materials. *Chem. Rev.* 121 (3), 1130–1202. doi:10.1021/acs.chemrev.0c00796

Nikelski, T., Schäfer, M. C., and Schleid, T. (2008). $La_4B_{14}O_{27}$: Ein Lanthan-ultra-Oxoborat mit Raumnetzstruktur. *Z. Für Anorg. Und Allg. Chem.* 634 (1), 49–55. doi:10.1002/zaac.200700303

Petříček, V., Dušek, M., and Palatinus, L. (2014). Crystallographic computing system JANA2006: General features. *Z. Für Kristallogr. - Cryst. Mater.* 229 (5), 345–352. doi:10.1515/zkri-2014-1737

Prescher, C., and Prakapenka, V. B. (2015). Dioptas: a program for reduction of two-dimensional X-ray diffraction data and data exploration. *High Press. Res.* 35 (3), 223–230. doi:10.1080/08957959.2015.1059835

Putz, H., and Brandenburg, K. (1999). *Diamond - crystal and molecular structure visualization.*

Rigaku Oxford Diffraction (2019). CrysAlisPro software system. Version 1.171.40.84a.

Rivers, M., Prakapenka, V., Kubo, A., Pullins, C., Holl, C., and Jacobsen, S. (2008). The COMPRES/GSECARS gas-loading system for diamond anvil cells at the Advanced Photon Source. *High Press. Res.* 28 (3), 273–292. doi:10.1080/08957950802333593

Sari, S., Senberber, F. T., Yildirim, M., Kipcak, A. S., Yuksel, S. A., and Derun, E. M. (2017). Lanthanum borate synthesis via the solid-state method from a La_2O_3 precursor: Electrical and optical properties. *Mater. Chem. Phys.* 200, 196–203. doi:10.1016/j.matchemphys.2017.07.056

Scott, W. D. (1962). Purification, growth of single crystals, and selected properties of MgF_2. *J. Am. Ceram. Soc.* 45 (12), 586–587. doi:10.1111/j.1151-2916.1962.tb11065.x

Sha, H., Li, B., Xiong, Z., Wang, Z., Liu, C., Su, R., et al. (2021). A new rare-earth borate birefringent crystal with quasi-two-dimensional $[BO_3]$ layers. *J. Mater. Chem. C* 9 (44), 15886–15890. doi:10.1039/D1TC04256D

Sheldrick, G. M. (2015). Shelxt – integrated space-group and crystal-structure determination. *Acta Crystallogr. Sect. A Found. Adv.* 71 (1), 3–8. doi:10.1107/S2053273314026370

Shmyt'ko, I. M., Kiryakin, I. N., and Strukova, G. K. (2013). Features of $LaBO_3$ phase formation during solid-phase synthesis from the amorphous precursor state. *Phys. Solid State* 55 (7), 1468–1475. doi:10.1134/S1063783413070305

Solntsev, V. P., Tsvetkov, E. G., Gets, V. A., and Antsygin, V. D. (2002). Growth of α-BaB_2O_4 single crystals from melts at various compositions: comparison of optical properties. *J. Cryst. Growth* 236 (1–3), 290–296. doi:10.1016/S0022-0248(01)02216-3

Solozhenko, V. L., Kurakevych, O. O., Le Godec, Y., and Brazhkin, V. V. (2015). Thermodynamically consistent p-T phase diagram of boron oxide B_2O_3 by *in situ* probing and thermodynamic analysis. *J. Phys. Chem. C* 119 (35), 20600–20605. doi:10.1021/acs.jpcc.5b07088

Toby, B. H., and Von Dreele, R. B. (2013). GSAS-II: the genesis of a modern open-source all purpose crystallography software package. *J. Appl. Crystallogr.* 46 (2), 544–549. doi:10.1107/S0021889813003531

Towns, J., Cockerill, T., Dahan, M., Foster, I., Gaither, K., Grimshaw, A., et al. (2014). Xsede: Accelerating scientific discovery. *Comput. Sci. Eng.* 16 (5), 62–74. doi:10.1109/MCSE.2014.80

Wang, F., Huber, L., Maehrlein, S. F., and Zhu, X.-Y. (2021a). Optical anisotropy and phase transitions in lead halide perovskites. *J. Phys. Chem. Lett.* 12 (20), 5016–5022. doi:10.1021/acs.jpclett.1c00918

Wang, V., Xu, N., Liu, J.-C., Tang, G., and Geng, W.-T. (2021b). Vaspkit: A user-friendly interface facilitating high-throughput computing and analysis using VASP code. *Comput. Phys. Commun.* 267, 108033. doi:10.1016/j.cpc.2021.108033

Wu, B.-L., Hu, C.-L., Mao, F.-F., Tang, R.-L., and Mao, J.-G. (2019). Highly polarizable Hg^{2+} induced a strong second harmonic generation signal and large birefringence in $LiHgPO_4$. *J. Am. Chem. Soc.* 141 (26), 10188–10192. doi:10.1021/jacs.9b05125

Wu, B., Tang, D., Ye, N., and Chen, C. (1996). Linear and nonlinear optical properties of the $KBe_2BO_3F_2$ (KBBF) crystal. *Opt. Mater.* 5 (1–2), 105–109. doi:10.1016/0925-3467(95)00050-X

Zhang, C., Divitt, S., Fan, Q., Zhu, W., Agrawal, A., Lu, Y., et al. (2020). Low-loss metasurface optics down to the deep ultraviolet region. *Light Sci. Appl.* 9 (1), 55. doi:10.1038/s41377-020-0287-y

Zou, G., and Ok, K. M. (2020). Novel ultraviolet (UV) nonlinear optical (NLO) materials discovered by chemical substitution-oriented design. *Chem. Sci.* 11 (21), 5404–5409. doi:10.1039/D0SC01936D